This is a repository copy of *Intracranial Aneurysm Detection from 3D Vascular Mesh Models with Ensemble Deep Learning*.

White Rose Research Online URL for this paper:
http://eprints.whiterose.ac.uk/160602/

Version: Accepted Version

Proceedings Paper:

Intracranial aneurysms detection in 3D cerebrovascular mesh model with ensemble deep learning

No Author Given

No Institute Given

Abstract. The intracranial aneurysms rupture can cause serious stroke, which relates to decline of daily life ability in the elderly. Although deep leaning is now the most successful solution for the organ detection, it requires myriads of training data, the consistency of image format and the balance of the sample distribution. This research innovatively presents the intracranial aneurysm detection problem as a shape analysis problem rather than a computer vision problem. We detect the intracranial aneurysms in 3D cerebrovascular mesh models after the segmentation of the brain vessel from the medical images, which can break the barriers of the data format and data distribution, serving both in clinical and screening. Also we propose a transferable multi-model ensemble (MMEN) architecture to detect the intracranial aneurysms from cerebrovascular mesh models with limited data. To obtain a well-defined convolution operator, we use the global seamless parameterization converting a 3D cerebrovascular mesh model to a planar flat-torus. In the architecture, we transfer the planar flat-torus presentation abilities of three GoogleNet Inception V3 models, which were pre-trained on the ImageNet database, to characterize the intracranial aneurysms with local and global geometric features such as Gaussian curvature, shape diameter function and WKS, respectively. We jointly utilize all these five models to detect aneurysms with adaptive weights learning based on back propagation. Experimental results on the 121 models show that our proposed method can achieve detection accuracy of 95.1% with 94.7% F1 score and 94.8% sensitivity, which is as good as the state-of-art work but applicable to inhomogeneous image modalities and smaller datasets.

1 Introduction

Severe stroke is most often caused by the rupture of intracranial aneurysms (IAs) [9]. Early detecting and quantifying IAs is essential for the prevention and treatment of aneurysm rupture and cerebral infarction. But detection, or identification of intracranial aneurysms is challenging due to the complexity and variability of their shapes. The location, the shape boundary and the size of IAs in population are quite different. Previous algorithm detected IAs using traditional machine learning method combined hand-craft features with enhancement filter, as blobness and vesseless filters, applied on medical images [7]. More recently, deep learning, particularly the deep convolutional neural network (DCNN), has become the most successful technique in IAs detection and it provides a unified framework for joint feature extraction and detection. Jerman [4] first utilized 7 layer 2D CNN to detect IAs with intra-vascular distance map. Nakao [10] utilized 6 layer 2D CNN on 9 direction MIP images of each

cube VOI. Ueda [16] applied ResNet-18 on 4 different types of parameters from TOF-MRA, which extended IAs detection works to multi-parameter images. Sichtermann [12] utilized "DeepMedic" with 2 pathways 11 layers network to deal both 3T and 1.5T 3D TOF-MRA together. Jin [5] detected IAs with 2D-DSA sequences combining U-net and BiConvLSTM. In previous works based on hand-craft feature selection, curvature, Hessian matrix, writhe number, skeleton information, and spherical harmonics function have been used to describe the boundary shape of the sphere-like aneurysms shape, while illumination and texture have been scarcely used, which shows that IAs detection problem is a graph problem rather than a vision problem. A major difference between traditional and deep learning methods is that traditional methods rely more on the domain knowledge such as sphere-like shape, whereas deep learning relies on access to massive datasets. Ideally, the advantages of both methods should be combined.

There are two limits in all previous works. First, there coexist different selection criteria for different image modalities. For example, CTA and 3DRA containing IAs are often used in clinic, while MRI without IAs is often used in targeted screening in population. This causes an imbalance of the sample distribution in each medical image modality. Second, due to economics and ethics reasons, the acquisition of large enough number of images as training data for the direct application of deep learning is prohibitive. In this paper we construct comparable 3D cerebrovascular models from any of the 3D image modalities, with which we can deal with different kinds of medical images and partially solve the data imbalance problem. We propose a transferable multi-model ensemble network (MMEN) for IAs detection from the cerebrovascular models. We then apply deep learning to the 3D mesh model with well-defined convolution operator on a global seamless parameterization to transfer the 3D cerebrovascular model to a planar flat-torus [6]. Three types of seamless counter-clockwise covers are designed to fine-tune pre-trained GoogleNet Inception V3 models (V3 models) [14], palliating the need for large data sets, with which we aimed to characterize the overall appearance of IAs in 3D mesh models. These V3 models are used jointly to detect IAs with an adaptive weighting scheme learned during the error back propagation, which enables the cerebrovascular mesh model to be trained in an *end-to-end* manner. The proposed method allows us to bridge the gap of different data format, break the barrier of the imbalance of the sample distribution and obtain enough training data. Compared to state-of-the art methods, our results show that the proposed algorithm provides substantial performance improvement.

2   Methods

The proposed MMEN algorithm is summarized in Fig. 1. The algorithm has four steps: (1) constructing the conformal mapping from input cerebrovascular mesh model S to the sphere-like surface S' and then conformal mapping from S' to planar flat-torus τ with seamless counter-clockwise covers of S' (2) building a MMEN architecture for 3D mesh model based classification (3) training the MMEN with the input dataset $\{S_i\}$ described with d-dimensional features until convergence, and (4) detecting IAs in each model based on the labels of aneurysms.
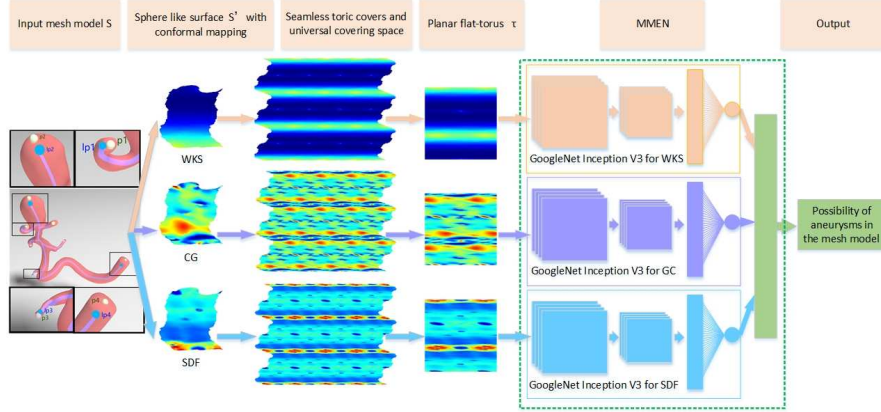
Fig. 1. Framework of our proposed MMEN algorithm.

Problem formulation Each 3D cerebrovascular structure can be modeled as a series of connected tubular-like 3D branches model. Our aim is to detect whether the IAs are in the 3D cerebrovascular model or not. The training data consist of a set of triplets $\{(S_i, \mathbf{x}_i, \hat{z}_i)\}_{i \in I}$ with 2D cerebrovascular watertight manifold models embedded in a three-dimensional space, $S_i \subset \mathbb{R}^3$, d-dimensional vector valued functions over the surface, $\mathbf{x}_i \in f(S_i, \mathbb{R}^d)$, and ground truth labeling functions $\hat{z}_i \in g(S_i, L)$, where $L = \{0, 1\}$ is the label set. Our goal is to find a non-linear mapping function as $F : f(S_i, \mathbb{R}^d) \to g(S_i, L)$ to produce a vector of confidences $F(\mathbf{x}_i) \in L$ per model S_i that correctly predicts its ground-truth label $\hat{z}_i$. Though the CNN is a powerful tool, existing architectures cannot directly run over S_i. We propose a transfer function to a planar flat-torus, denoted as τ, and train a CNN over τ with traditional 2D convolution operator on τ discretized in a grid. The key component is mapping S to τ, which is a not trivial problem for the different topology between S and τ.

Seamless parameterization and convolution operator We define a sphere-like surface S' as an intermediate surface to create a desired seamless map between S and image τ. For given quarter-points $P = \{p_1, p_2, p_3, p_4\}$, we can obtain a unique transfer operation along the path $p_1 \to p_2 \to p_3 \to p_4$ to obtain the torus-like surface S'. Then we construct the universal covering space through stitching the surface S' with the method in [1] duplicating the planar mesh until we cover the representative square tile of the planar flat-torus with the orbifold as $\{\pi, \pi, \pi, \pi\}$. We use the cotan weights with negative values clamped to 10^{-2} to ensure positivity and hence bijective mapping. The quarter-points P can be computed very efficiently of the approximated-conformal map by solving a sparse system of linear equation. We use ϕ_P as the transfer function between the sphere-like surface S' and the flat-torus τ, its push-forward to the flat image is defined as $\text{push}_P(x) = x \circ \varphi \circ \phi_P^{-1}$, where φ is the projection map from S' to S. We evaluate x at that point and assign the corresponding d-dimensional feature vector to it.

The convolution operator on the surface S requires to be translation invariant. First, the definition of the map $S \to S'$ guarantees that a translation on S' is a local Euclidean translation on S. Second, according to Poincaré-Hopf Theorem [8], for

closed orientable surfaces, only torus-like surfaces, whose Euler characteristic is zero, has non-vanishing vector fields. Given two closed surfaces: S' (sphere-liked) and τ (planar flat-torus) with a conformal homeomorphism $\phi : S' \rightarrow \tau$, a convolution operator $*_{(\tau)}$ on τ defines a corresponding convolution operator on S', by $f *_{(S')} g = ((f \circ \phi^{-1}) *_{(\tau)} (g \circ \phi^{-1})) \circ \phi$. As the convolution on the planar flat-torus τ is invariant to Euclidean translations σ, the convolution on S' is invariant to its translation $\phi^{-1} \circ \sigma \circ \phi$. Since the ϕ^{-1}, σ and ϕ are all conformal maps, these translations are also conformal maps. This means that no previous alignment on the cerebrovascular model is needed in this work.

Data and materials generation. The used database gathers the 3D model reconstruction resulting from a series of medical images of different modalities, in which the location and presence of aneurysms were evaluated by up to four experienced thoracic radiologists. The positive dataset (with aneurysms) of 56 patients is drawn from a large multicenter database created within the EU-funded project @neurIST [17] based on the 3DRA image. The negative dataset (without aneurysms), derived from the public dataset distributed by the MIDAS Data Server at Kitware Inc. [2], contains 50 MRAs of the cerebral vascular from healthy volunteers. Since MRA images includes a larger portion of the cerebral vasculature than 3DRA, we selected only segments with branches similar to the ones present in the 3DRA mesh models, such as the anterior cerebral artery (ACA) or the internal carotid artery (ICA) bifurcation. No other information was considered during the selection process.

To train the network, we first need to push the training data to images defined over the planar flat-torus τ with seamless counter-clockwise covers. Given the training data $\{(S_i, x_i, \hat{z}_i)\}_{i \in I}$, for each i we sample ρ quarter-points $P = \{p_1, p_2, p_3, p_4\} \subset S_i$. The skeleton of the vascular model is computed by the method in [15], and each skeleton endpoint is related to the corresponding vertices of the mesh model. The longest road in the skeleton is identified and its two endpoints are labeled as lp_1 and lp_4. The endpoint with largest number of binding vertices (likely representing a big aneurysm), excluding lp_1 and lp_4, is labeled as lp_2. A fourth point lp_3 is identified as the endpoint with the shortest skeleton length to lp_1 or lp_4. In case the skeleton only has three branches, we set lp_3 equal to lp_2. Then, each point p_i is randomly selected (without repetition) from the binding points of lp_i. This choice of quarter-points follow the rationale of well-covering the surface to allow each point to be represented with a reasonable scale factor at least in one map. Hence we sampled a small number (in practice, $\rho = 10$) of uniformly spread points P on the surface. We cut the square flat-image τ from the universal covering space with sphere-like surface S'. To avoid the data similarity, we set the random cut in their universal covering space with sphere-like surface S' computed with different points P, for their close positions. The number of training samples can be increased by data augmentation, which can play an important role in deep learning with small data sets. We used a 6x data augmentation in our experiments with mirroring, rotation and flipping operations.

Feature selection. The conformal mapping can only convert the 3D mesh model S to the flat image τ with smallest twist. Different kind of features must be used to describe the shape of the models. Our map provides a relatively small space of possible parameterizations, which make learning easier. For the local features, we

choose the shape diameter function (SDF) and Guassian curvature (GC) of each point in the model. For the global features, we use the spectral decomposition of Laplace-Beltrami operator on manifold to create spectral shape descriptors: wave kernel signature (WKS). We use the multi-model neural network to aggregate all these three feature maps.

Multi-model ensemble neural network on the planar flat-torus τ. We present a multi-model ensemble architecture with cerebral mesh models to three-dimensional features on τ. The V3 model pre-trained on the ImageNet dataset is adopted with one fully connected (FC) layer (GV3F) as the fundamental classifier for each feature image on τ. Three copies of this GoogleNet are fine-tuned using the input of three-dimensional features on τ in Fig.1. The output neurons in the last fully connected layer of the classifiers are connected with one fully connected layer (MMEN) to give the final decision. This architecture is a non-linear function taking three-dimensional functions over the image τ to L valued functions over the image which can be defined as $F(, \mathbf{w}) : \mathbb{R}^{m \times n \times 3} \to \mathbb{R}^{m \times n} \times L$.

A two-step training is used in the architecture. For each classifier, the loss function is defined as binary cross entropy $E(w) = - \sum_k \left[\hat{z}_i \log(p(x_i^b)) + (1 - \hat{z}_i) \log(1 - p(x_i^b)) \right]$. We use stochastic gradient decent method with batch size of 128 and learning rate of 0.01. The initial weights are stochastically selected with a truncated normal Gaussian distribution in $[-1, 1]$. We stop training when the total loss is less than 0.2 for 500 iterations. When all the features are stably trained on τ, we begin the multi-model ensemble architecture training. $p(x_i^b)$ denotes the prediction result by b-th GoogleNet result, the ultimate prediction result of the ensemble model is calculated as $P_i = \sum_{j=1}^b w_{ij} p(x_i^b)$, where P_i is the likelihood of the input model belonging to category $L \in \{0, 1\}$. The binary cross entropy loss function is used again in this ensemble model, and the change of weight is $\Delta w = -\eta(\sum_i \frac{\hat{z}_i}{P_i} - (\frac{1 - \hat{z}_i}{1 - P_i}))$, for the learning rate $\eta = 0.01$. Stochastic gradient decent with a bath size 64 is adopted due to our small number of training data. A 5-fold cross validation is used, where 5% of the traning models are chosen as validation set in each fold. The training is terminated even before reaching the maximum iteration number of 1000.

3   Experiments

We conduct our research platform based on TensorFlow using an NVIDIA 960 M GPU on an Ubuntu 16.10 Linux OS 64-bit operating system. The proposed MMEN architecture has been applied to the dataset 5 times independently, with 5-fold cross validation. The mean and standard deviation of the obtained false positive ratio, specificity, accuracy and sensitivity in the full data set is presented in Table 1 and compared with the performance of 6 state-of-the-art methods with different data sets. Our results are superior in some of the metrics, depending on the compared study, although a more global and direct comparison is hindered by the differences in data sets and evaluation criteria. Our algorithm obtain similar or superior results to both hand-crafted feature-based traditional methods and other deep leaning methods [12, 16, 5, 10, 4], which requires more homogeneous data formats. Our results indicate that (1) conformal parameterization method provides a valid mesh representation, (2)

pre-trained and fine-tuned V3 model can effectively transfer the image representation ability learned on the ImageNet dataset to characterize the parameterization method model, (3) an adaptive ensemble of these images has superior ability in identifying aneurysms in cerebrovascular mesh models.

Table 1. Comparison of the performance of out proposed method to 6 state-of-the-art aneurysms detection methods on different data set. *I: input data format; N: number of cases; F: false positive ratio; S: Specificity; A: Accuracy; SE: Sensitivity;*

Algorithms	I	N	F	S (%)	A (%)	SE (%)
Sichtermann, *et al.* 19 [12]	3D TOF-MRA (1.5T,3T)	85	8.14	poor	-	87
Ueda, *et al.* 19 [16]	3D TOF-MRA (1.5T,3T)	748	10	-	-	91
Jin, *et al.*19 [5]	2D-DSA	493	3.77	-	-	89.3
Nakao, *et al.*18 [10]	3D TOF-MRA (3T)	450	2.9	-	-	94.2
Jerman, *et al.*17 [4]	3D-DSA	15	2.4	-	95	100
MIKI,*et al.* 16 [7]	3D MRI(3T)	2701	-	-	-	82
Proposed (Mean ± standard deviation)	3DRA+3D TOF MRI(1.5T)	**121**	**0.8±0.6**	**95.4±6.2**	**95.1±4.0**	**94.8±6.7**

4 Discussion

Different parameterization method The parameterization of the mesh model S plays an important role in applying a deep model on the 3D mesh model problem. On one hand, the conformal mapping from S to τ provides the parameterization involving the least twist. On the other hand, the computational complexity of our method is also small. We re-performed the experiments using different kinds of parameterization methods. The obtained performances are listed in Table 2. AP is the index of the area changing in the parameterization. If the surface area ratio between the aneurysms part and the branch part is quite similar as the original, the area twist would be small, just like our method.

Table 2. Comparison of the performance of our conformal parametrization to such of the sphere parameterization [11] on 3D mesh models with aneurysms. *SP: sphere parameterization; M number of missing aneurysms in parameterization images of each cerebrovascular model; AP: surface area ratio between the aneurysms part and the branch part. R: running time for the parameterization. Mean ± standard deviation.*

Parameterization	M	AP(%)	R(s)
Orginal mesh model S	-	2.36 ± 0.48	-
SP [11]	3.90 ± 2.69	0.14 ± 0.14	104.072
Proposed	0	**1.77 ± 0.58**	**12.6**

Ensemble learning To demonstrate the performance improvement provided by the feature combination by the adaptive ensemble with respect to each of the three V3 models with independent features (WKS, GC and SDF), we compared their performance on the same data set of intracranial aneurysms (Table 3). Although each

V3 model achieves a relatively good performance, the adaptive ensemble of them achieves a better performance gain.

Table 3. Performance comparison of each component V3 model, considering only one feature, and the proposed MMEN model combining all of them. *T: training time(s);*

Models	A(%)	SE(%)	S(%)	P(%)	T(s)
V3 for WKS	82.6	91.2	75.4	76.9	29.8
V3 for GC	86.8	87.7	86.2	85.8	29.7
V3 for SDF	88.4	91.1	86.2	86.0	30.2
Proposed	**95.1**	**94.8**	**95.4**	**95.1**	**92.4**

Other Pre-trained DCNN Models Besides GoogLeNet, VGGNet [13] is also the most successful DCNN models. Using each of those two models to characterize each of the three features (WKS, GC and SDF), we have 8 different configurations. To evaluate the performance of using other DCNN models, we tested all these configurations. Table 3 shows the F1 score with sensitivities for the best five configurations. It shows that V3 model is very powerful, using three v3 models results in the highest F1 score with less training time and using two V3 model can also obtain the good results. Nevertheless, it also suggests that VGGNet are also good choices as well and using them to replace GoogLeNet may produce very similar good F1 score and sensitivities in some configurations. ResNet-50 [3] model results are shown in supplementary material for the space limits.

Table 4. Performance of top-5 models from 8 ensemble models. *F1: F1 score*

DNN for WKS	DNN for GC	DNN for SDF	F1(%)	SE(%)	T(s)
GoogLeNet	GoogLeNet	GoogLeNet	**94.7**	**94.8**	**92.4**
GoogLeNet	GoogLeNet	VGGNet	90.4	91.2	262.0
VGGNet	GoogLeNet	GoogLeNet	90.3	91.1	261.8
GoogLeNet	VGGNet	GoogLeNet	89.2	87.7	262.1
VGGNet	GoogLeNet	VGGNet	87.8	89.2	431.8

Other things: computational complexity and failed results In our experiments, it took about 92.4s to train the proposed model and less than 0.5s for aneurysms detection in each mesh model. It suggests that the proposed algorithm is very efficient for offline training and online testing. In the positive data set, models of 2, 10 and 50 with failed detection have the average diameter smaller than 4mm with irregular shape boundary, which is also very difficult for the radiologist to decide. Some more details on further aspects are described in the supplementary material.

5 Conclusion

We propose the MMEN algorithm to detect intracranial aneurysms in cerebrovascular mesh model from 3DRA data and MRA data. We seamless parameterize the

input mesh model to the planar flat-torus with universal covering space. We used three pre-trained and fine-tuned GoogleNet Reception V3 models to characterize the cerebrovascular mesh model with three geometrical features (WKS, SDF and GC), and combined these models using an adaptive weighting scheme learned during the back-propagation process. The results show that our algorithm produces more accurate results, having good potential as a novel IAs detection framework.

References

1. Y. Aigerman, N.and Lipman. Orbifold tutte embeddings. *TOG*, 34(6):1–12, 2015.
2. S.R. Aylward and E. Bullitt. Initialization, noise, singularities, and scale in height ridge traversal for tubular object centerline extraction. *TMI*, 21(2):61–75, 2002.
3. K. He, X. Zhang, and S. Ren et al. Deep residual learning for image recognition. In *CVPR*, pages 770–778, 2016.
4. T. Jerman, F. Pernus, and B. Likar et al. Aneurysm detection in 3D cerebral angiograms based on intra-vascular distance mapping and convolutional neural networks. In *ISBI*, pages 612–615, 2017.
5. H. Jin, Y. Yin, and M. Hu et al. Fully automated unruptured intracranial aneurysm detection and segmentation from digital subtraction angiography series using an end-to-end spatiotemporal deep neural network. In *SPIE Medical Imaging 2019*, pages 1–8, 2019.
6. H. Maron, M. Galun, and N. Aigerman et al. Convolutional neural networks on surfaces via seamless toric covers. *TOG*, 36(4):71–1, 2017.
7. S Miki, N Hayashi, and Y Masutani et al. Computer-assisted detection of cerebral aneurysms in mr angiography in a routine image-reading environment: effects on diagnosis by radiologists. *AJNR*, 37(6):1038–1043, 2016.
8. J.W. Milnor and D.W. Weaver. *Topology from the differentiable viewpoint*. Princeton university press, 1997.
9. D. Mozaffarian, E.J. Benjamin, and A.S. Go et al. Executive summary: Heart disease and stroke statistics-2016 update: A report from the american heart association. *Circulation*, 133(4):447–454, 2016.
10. T. Nakao, S. Hanaoka, and Y. Nomura et al. Deep neural network-based computer-assisted detection of cerebral aneurysms in MR angiography. *JMRI*, 47(4):948–953, 2018.
11. E. Praun and H. Hoppe. Spherical parametrization and remeshing. *TOG*, 22(3):340–349, 2003.
12. T Sichtermann, A Faron, and R Sijben et al. Deep learning-based detection of intracranial aneurysms in 3D TOF-MRA. *AJNR*, 40(1):25–32, 2019.
13. K. Simonyan and A. Zisserman. Very deep convolutional networks for large-scale image recognition. *arXiv:1409.1556*, 2014.
14. C. Szegedy, W. Liu, and Y. Jia et al. Going deeper with convolutions. In *CVPR*, pages 1–9, 2015.
15. A. Tagliasacchi, I. Alhashim, and M Olson et al. Mean curvature skeletons. *CGF*, 31(5):1735–1744, 2012.
16. D. Ueda, Yamamoto A., and M. Nishimori. Deep learning for MR angiography:automated detection of cerebral aneurysms. *Radiology*, 290:187–194, 2019.
17. M.C. Villa-Uriol, G. Berti, and D.R. Hose et al. @ neurist complex information processing toolchain for the integrated management of cerebral aneurysms. *Interface Focus*, 1(3):308–319, 2011.